Hydrol. Earth Syst. Sci. Discuss., 10, 15771–15809, 2013
www.hydrol-earth-syst-sci-discuss.net/10/15771/2013/
doi:10.5194/hessd-10-15771-2013

Hydrology and Earth System Sciences
Open Access
Discussions

Modelling stream flow and quantifying blue water using modified STREAM model in the Upper Pangani River Basin, Eastern Africa

J. K. Kiptala[1,2], **M. L. Mul**[1,3], **Y. Mohamed**[1,4,5], **and P. van der Zaag**[1,4]

[1]UNESCO-IHE, Institute for Water Education, P.O. Box 3015, 2601 DA Delft, the Netherlands
[2]Jomo Kenyatta University of Agri. and Technology, P.O. Box 62000, 00200 Nairobi, Kenya
[3]International Water Management Institute, PMT CT 112, Cantonments, Accra, Ghana
[4]Delft University of Technology, P.O. Box 5048, 2600 GA Delft, the Netherlands
[5]Hydraulic Research Station, P.O. Box 318, Wad Medani, Sudan

Received: 25 October 2013 – Accepted: 11 December 2013 – Published: 23 December 2013

Correspondence to: J. K. Kiptala (j.kiptala@unesco-ihe.org, kiptalajeremy@yahoo.com)

Published by Copernicus Publications on behalf of the European Geosciences Union.

Abstract

Effective management of all water uses in a river basin requires spatially distributed information of evaporative water use and the link towards the river flows. Physically based spatially distributed models are often used to generate this kind of information. These models require enormous amounts of data, if not sufficient would result in equifinality. In addition, hydrological models often focus on natural processes and fail to account for water usage. This study presents a spatially distributed hydrological model that has been developed for a heterogeneous, highly utilized and data scarce river basin in Eastern Africa. Using an innovative approach, remote sensing derived evapotranspiration and soil moisture variables for three years were incorporated as input data in the model conceptualization of the STREAM model (Spatial Tools for River basin Environmental Analysis and Management). To cater for the extensive irrigation water application, an additional blue water component was incorporated in the STREAM model to quantify irrigation water use ($ET_{b(I)}$). To enhance model parameter identification and calibration, three hydrological landscapes (wetlands, hill-slope and snowmelt) were identified using field data. The model was calibrated against discharge data from five gauging stations and showed considerably good performance especially in the simulation of low flows where the Nash–Sutcliffe Efficiency of the natural logarithm (E_{ln}) of discharge were greater than 0.6 in both calibration and validation periods. At the outlet, the E_{ln} coefficient was even higher (0.90). During low flows, $ET_{b(I)}$ consumed nearly 50 % of the river flow in the river basin. $ET_{b(I)}$ model result was comparable to the field based net irrigation estimates with less than 20 % difference. These results show the great potential of developing spatially distributed models that can account for supplementary water use. Such information is important for water resources planning and management in heavily utilized catchment areas. Model flexibility offers the opportunity for continuous model improvement when more data become available.

HESSD
10, 15771–15809, 2013

1 Introduction

Hydrological models are indispensible for water resource planning at catchment scale as these can provide detailed information on, for example, impacts of different scenarios and trade-off analyses. Society's demand for more accountability in the management of externalities between upstream and the downstream water users has also intensified the need for more predictive and accurate models. However, complexity of hydrological processes and high levels of heterogeneity present considerable challenges in model development. Such challenges have been exacerbated over time by land use changes that have influenced the rainfall partitioning into *green* (soil moisture) and *blue* (runoff) water resources. In spite of these challenges, it is desirable to develop a distributed hydrological model that can simulate the dominant hydrological processes and take into account the various water uses. In large catchments with high heterogeneity, key variables such as water storage (in unsaturated and saturated zones) and evaporation (including transpiration) are difficult to obtain directly from point measurements. This becomes even more difficult for ungauged or poorly gauged river basins.

In most cases those variables are derived from models using (limited) river discharge data which increases equifinality problems (Savenije, 2001; Uhlenbrook et al., 2004; McDonnell et al., 2007; Immerzeel and Droogers, 2008). On the other hand, grid based distributed models at fine spatial scales do not account for additional *blue water* use (ET_b), i.e. transpiration from supplementary irrigation or withdrawals from open water evaporation. In fact in tropical arid regions, ET_b (during low flows) can be a large percentage of the river discharge. This may lead to high predictive uncertainty in the hydrological model outputs especially when dealing with scenarios for water use planning in the catchments.

To overcome these challenges, many researchers have opted for simple, lumped and or parsimonious models with a limited number of model parameters. The models are simplified by bounding and aggregation of some functionality in the complex system

HESSD
10, 15771–15809, 2013

(Winsemius et al., 2008). In doing so, models may become too simplified to represent hydrological processes in a catchment (Savenije, 2010). Therefore, Savenije (2010) proposes a conceptual model mainly based on topographic characteristic to represent the dominant hydrological processes. The model maintains the observable landscape characteristics and requires a limited number of parameters. Other researchers have used secondary data, e.g. from remote sensing to calibrate or infer model parameters as much as possible (Winsemius et al., 2008; Immerzeel and Droogers, 2008; Campo et al., 2006). This has been possible in the recent past because of the availability of images of finer spatial resolutions from a variety of satellite images. Advancement in remote sensing algorithms has also resultant in wider range spatial data of reasonably good accuracies. Such spatial data include actual evapotranspiration (ET_a) derived from remote sensing applications, e.g. TSEB (Norman et al., 1995), SEBAL (Bastiaanssen et al., 1998a, b), S-SEBI (Roerink et al., 2000), SEBS (Su, 2002) and METRIC (Allen et al., 2007). Spatial data on soil moisture can also be derived from satellite images, e.g. from ERS-1 Synthetic Aperture Radar (SAR) combined with the TOPMODEL topographic index (Scipal et al., 2005) or from Moderate-resolution Imaging Spectroradiometer (MODIS) combined with the SEBAL model (Mohamed et al., 2004). It is also evident that distributed models perform well with finer resolution data as demonstrated by Shrestha et al. (2007). Using different resolution data (grid precipitation and grid ET_a) and a concept of IC ratio (Input grid data area to Catchment area) they found that a ratio higher than 10 produces a better performance in the Huaihe River Basin and its sub-basin of Wangjiaba and Suiping in China.

Furthermore, remotely sensed data at finer resolutions offer great potential for incorporating blue water, in the form of (supplementary) irrigation water ($ET_{b(I)}$) in model conceptualization. This opportunity arises from the fact that remote sensed ET_a based on energy balance provides total evaporation that already accounts for the additional blue ET_b. For instance, Romaguera et al. (2012) used the difference between Meteosat Second Generation (MSG) satellites data (total ET_a) and Global Land Data Assimilation System (GLDAS) which does not account for ET_b, to quantify blue water use for

HESSD
10, 15771–15809, 2013

croplands in Europe with a reasonable accuracy. However, the spatial scales of such datasets (GLDAS (1 km) and MSG (3 km)) limit the application. Nevertheless, the latter recommends the concept application to recently available data of wider spatial and temporal coverage, e.g. data derived from MODIS 250 m, 500 m.

However, the literature shows limited applications of utilizing grid data for distributed hydrological models in poorly gauged catchments. Winsemius et al. (2006) showed that the soil moisture variations from the Gravity Recovery And Climate Experiment (GRACE) could provide useful information to infer and constrain hydrological model parameters in the Zambezi river basin. Campo et al. (2006) using an algorithm developed by Nelder and Mead (1965), used remotely sensing soil moisture information to calibrate a distributed hydrological model in the Arno basin, Italy. Immerzeel and Droogers (2008) used remotely sensed ET_a derived from SEBAL in the calibration of a Soil and Water Assessment Tool (SWAT) model of the Krishna basin in southern India in which the model performance (r^2) increased from 0.40 to 0.81.

The factors that may have limited the application of this technique include: (a) limited flexibility of hydrological models to utilize spatially distributed data. This is normally the case where the user has no control over the model source code. The user is therefore limited to optimizing model performance using secondary data. (b) Limited availability of accurate data at the proper spatial and temporal scales to capture dominant hydrological processes in a catchment. Furthermore, the procedure used to derive relevant information from satellite images is time consuming. This is exacerbated when generating time series of spatial data from images with clouds.

This paper presents a novel method of using of ET_a and soil moisture data derived from satellite images as input in a distributed hydrological model. The Upper Pangani River Basin in Eastern Africa has been used as a case study. This river basin has heavily managed landscapes dominated by irrigated agriculture. The secondary data used in this study have been generated using MODIS satellite information and the SEBAL model on 250 m and 8 day resolutions for the period 2008–2010 (Kiptala et al., 2013b). Here the STREAM model has been modified to incorporate blue water use.

HESSD
10, 15771–15809, 2013

The model parameters have also been limited further by the topographic characteristics and groundwater observations using the hydrological conceptualization developed by Savenije (2010).

2 Study area

The Upper Pangani River Basin (13 400 km^2) covers approximately 30 % of the total area of the Pangani River Basin (Fig. 1). It is the main headwaters of the basin and derives its water sources from the Mt. Kilimanjaro (5880 m a.s.l.) and Mt. Meru (4565 m.a.s.l) catchments. The flows to the lower basin are regulated by a large dam (storage capacity 1100 Mm^3), the Nyumba ya Mungu (NyM) reservoir. The Lower Pangani River Basin has three operational hydro-electric power (HEP) stations: NyM HEP, Hale HEP and the New Pangani Falls HEP stations. These provide up to 91.5 MW or 17 % of Tanzania's electricity.

The catchment has a highly varied climate mainly influenced by topography. The high altitude slopes around the mountain ranges have an Afro-Alpine climate and receive nearly 2500 mm yr^{-1} of rainfall. The lower parts have a sub-humid to semi-arid climate and the rainfall varies between 300 to 800 mm yr^{-1}. The rainfall has a bimodal pattern where long rains are experienced in the months of March to May (*Masika* season) and the short rains in the months of November and December (*Vuli* season). It is during these two seasons when most crops are grown. Rainfed and supplementary irrigated croplands are the dominant agricultural systems. However, grasslands and shrublands are also dominant land use types (see Sect. 3.2).

HESSD
10, 15771–15809, 2013

3 Materials and methods

3.1 Hydro-meteorological data

Daily rainfall data for 93 stations located in or near the Upper Pangani River Basin were obtained from the Tanzania Meteorological Agency and the Kenya Meteorological Department. However, only 43 stations proved useful after data validation for the period 2008–2010. Unfortunately, there are no rainfall stations at elevations higher than 2000 m a.s.l. where the highest rainfall actually occurs. Remote sensed sources of rainfall data based on or scaled by ground measurements have similar shortcoming, e.g. FEWS and TRMM. According to PWBO/IUCN (2006), the maximum mean annual precipitation (MAP) at the Pangani River Basin is estimated at 3453 mm yr^{-1} that is estimated to occur at elevation 2453 m a.s.l. Therefore, a linear extrapolation method based on the concept of double mass curve was used to derive the rainfall up to the mountain peaks using the rainfall data from the neighbouring stations. It was assumed that the MAP is constant above this elevation to 4565 m a.s.l. for Mt. Meru and 5880 m a.s.l. for Mt. Kilimanjaro. This assumption is expected to have negligible effect at the Pangani River Basin because of the relative small area above this elevation. Six dummy stations were therefore extrapolated from the existing rainfall stations to the mountain peaks.

River discharges for six gauging stations were obtained from the Pangani Basin Water Office (Moshi, Tanzania), see Fig. 1. The measurements were obtained as daily water level measurements and converted to daily discharge data using their corresponding rating curves equations for the period 2008–2010. The actual evapotranspiration (ET_a) and soil moisture data for the Upper Pangani River Basin were obtained from a recent and related research by Kiptala et al. (2013b). ET_a and soil moisture data for 8 day and 250 m resolutions for the years 2008–2010 were derived from MODIS satellite images using the Surface Energy Balance Algorithm of Land (SEBAL) algorithm (Bastiaanssen et al., 1998a, b).

HESSD
10, 15771–15809, 2013

3.2 Land use and land cover types

In this study, we employed the LULC classification for the Upper Pangani River Basin from a recent research by Kiptala et al. (2013a). They derived the LULC types using phenological variability of vegetation for the same period of analysis, 2008 to 2010. LULC types include 16 classes dominated by rainfed maize and shrublands that constitute half of the area in the Upper Pangani River Basin.

3.3 Other spatial data

Elevation and soil information were also obtained for the Upper Pangani River Basin. A digital Elevation Model (DEM) with 90 m resolution was obtained from the Shuttle Radar Topography Mission (SRTM) of the NASA (Farr et al., 2007). The soil map was obtained from the harmonized world soil database which relied on soil and terrain (SOTER) regional maps for Northern and Southern Africa (FAO/IIASA/ISRIC/ISSCAS/JRC, 2012).

3.4 Model development

The hydrological model was built to simulate stream flow for the period 2008–2010 for the Upper Pangani River Basin. An 8 day timestep and 250 m moderate resolutions has been used to correspond to the remotely sensed secondary data for the same period of analysis. The 8 day timestep generally corresponds to the time scale that characterizes agricultural water use. In addition, this timescale is assumed to be sufficiently large to neglect travel time lag in the river basin. The other general hydrological processes in the river basin are estimated to have larger time scales (Notter et al., 2012). The spatial scale of 250 m is limited by the available MODIS satellite data. This is reasonably representative of the sizes of the small-scale irrigation schemes in the Upper Pangani River Basin.

HESSD
10, 15771–15809, 2013

STREAM, a physically based conceptual model, is developed in the PcRaster modelling environment (Aerts et al., 1999). The PcRaster scripting model environment consists of a wide range of analytical functions for manipulating Raster GIS maps (Karssenberg et al., 2001). It uses a dynamic script to analyze hydrological processes in a spatial environment. The PcRaster environment allows for tailored model development and can therefore be used to develop new models, suiting the specific aims of the research including the availability of field data. The STREAM model in PcRaster environment allows the inclusion of spatially variable information like ET_a and soil moisture in the model. Furthermore, STREAM model is an open source model which has been applied successfully in other data limited river basins, especially in Africa (Gerrits, 2005; Winsemius et al., 2006; Abwoga, 2012; Bashange, 2013).

In the STREAM model, surface runoff is computed from the water balance of each individual grid cell, which is then accumulated in the local drainage direction derived from DEM to the outlet point (the gauging station). The model structure consists of a series of reservoirs where the surface flows are routed to the rivers using calibration coefficients. We modified the STREAM model by including an additional blue water storage parameter (S_b) that regulates ET_b in the unsaturated zone. ET_b can be derived from the groundwater as capillary rise, $C(t)$, or river abstraction, $Q_b(t)$. The input variables for the modified STREAM model are: Precipitation (P), Interception (I) calculated on a daily basis as a pre-processor outside the model, Transpiration (T_a) (ET_a (from SEBAL) – I) and $S_{u,min}$ (from SEBAL). The other parameters are calibration factors. Figure 2 shows the modified STREAM model structure for Upper Pangani River Basin.

In the model T_a and the $S_{u,min}$ are the main drivers of the hydrological processes in the unsaturated zone of the model. T_a is the soil moisture depletion component while $S_{u,min}$ is the depletion threshold. The unsaturated storage (S_u) is replenished by the component of net precipitation ($P_e \times C_r$) and ET_b from groundwater through capillary rise or river abstractions. It is assumed that excess water from the upstream cells or pixels would supplement water needs of the middle or lower catchments where supplementary water is used. This is a typical river basin where precipitation is higher

HESSD
10, 15771–15809, 2013

than ET_a in the upper catchments, which contributes water in the form of river flow to the downstream catchments.

The rationale for accounting for ET_b in the model is motivated by the failure of the original STREAM model to simulate actual transpiration in a realistic way. Bashange (2013) found that simulated T_a obtained from STREAM for irrigated croplands were significantly lower compared to SEBAL T_a($ET_a - I$) for dry seasons in the Kakiwe Catchment, Upper Pangani River Basin. The result was attributed to lower soil moisture levels at the unsaturated zone (not replenished in the model by blue water use). Bashange (2013) used the relation by Rijtema and Aboukhaled (1975) where the transpiration was derived only a function of potential evaporation and the soil moisture (from precipitation) in the unsaturated zone.

3.5 Model configuration

3.5.1 Model input

Interception (I)

When precipitation occurs over a landscape, not all of it infiltrates into the subsurface or becomes runoff. Part of it evaporates back to the atmosphere within the same day the rainfall takes place as interception. The interception consists of several components that include canopy interception, shallow soil interception or evaporation from temporary surface storage (Savenije, 2004). The interception is dependent on the land use and is modeled as a threshold value (D). The interception process is typically on a daily time scale, although some work has been done to parameterize the interception threshold on a monthly timescale (De Groen and Savenije, 2006).

In our case, we calculate the daily interception according to Savenije, (1997, 2004) outside of the model (see Eq. 1);

$$I_d = \min(D_d, P_d) \quad (1)$$

HESSD
10, 15771–15809, 2013

Where I_d is the daily interception, D_d daily interception threshold and P_d is the observed precipitation on a rainy day. Since I_d occurs on a daily time step during a precipitation (P_d) event, the interception at 8 day ($I_{d(8)}$) is derived from the accumulated daily interception computed based on daily precipitation. The Interception thresholds (D_d) vary per land use and have been adopted from the guidelines provided by Liu and de Smedt (2004) and Gerrits (2010). As such an interception threshold of 2.5 mm day^{-1} was used for croplands and natural vegetation and 4 mm day^{-1} for forest.

Net precipitation (P_e)

The net precipitation ($P_{e(8)}$) is calculated by subtracting the accumulated interception ($I_{d(8)}$) from the accumulated precipitation ($P_{d(8)}$) for the 8 day time scale.

$$P_{e(8)} = (P_{d(8)} - I_{d(8)}) \quad (2)$$

$P_{e(8)}$ is split through a separation coefficient, C_r into the two storages, unsaturated and saturated (groundwater) storages. C_r is a calibration factor that is dependent on the soil type and land use types.

Actual transpiration (T_a)

The transpiration (T_a) is also derived by subtracting the interception component of the actual evapotranspiration (ET_a) at each timestep. ET_a from SEBAL accounts for total evaporation (on 8 day timestep) that includes $I_{d(8)}$.

$$T_a = (ET_a - I_{d(8)}) \quad (3)$$

3.5.2 Unsaturated zone

The maximum soil moisture storage ($S_{u,max}$) was defined based on land use and soil types. Water available for transpiration includes water infiltrated from precipitation ($P_e \times C_r$) and water from capillary rise and irrigation, ET_b (discussed in the next section).

HESSD
10, 15771–15809, 2013

During the dry (nonrainy) periods, the spatial variation in soil moisture is controlled by vegetation through the uptake of blue water resources (Seyfried and Wilcox, 1995). The model assumes a minimum soil moisture level ($S_{u,min}$) which varies for managed and natural landscapes. Soil moisture is therefore a key variable controlling water and energy fluxes in soils (Eqs. 4 and 5).

$$ET_b = T_a \rightarrow \text{if } (S_u \leq S_{u,min}) \quad (4)$$

$$ET_b = 0 \rightarrow \text{if } (S_u > S_{u,min}) \quad (5)$$

The value for $S_{u,min}$ for each land use type is assumed to be realized during the dry months and is expressed as a fraction of $S_{u,max}$ (soil moisture depletion fraction). $S_{u,min}$ is derived in the SEBAL model for dry months as an empirical function of the evaporative fraction, Λ (the ratio of the actual to the crop evaporative demand when the atmospheric moisture conditions are in equilibrium with the soil moisture conditions) (Ahmed and Bastiaanssen, 2003), see Eq. (6).

$$f = \frac{S_{u,min}}{S_{u,max}} = e^{(\Lambda-1)/0.421} \quad (6)$$

where f is the soil moisture depletion faction expressed as a fraction of soil moisture, $S_{u,min}$ to the moisture value at full saturation, $S_{u,max}$ for the dry months. $S_{u,min}$ was realized in the months January, which is the driest period in the river basin. Values for f are given in Fig. 3 for selected land use types for dry month of January averaged over 2008–2010.

The soil moisture levels agree reasonably well with previous field studies that have shown similar ranges for natural land use types in sub humid and semi-arid areas (Fu et al., 2003; Korres et al., 2013). It is also noted that the SEBAL model has some level of uncertainty to soil moisture storage and water stress (Ruhoff et al., 2012). In recognizing this uncertainty, the modified SEBAL model also uses a water balance approach where lower $S_{u,min}$ levels can be tolerated with respect to the available Q_b during the dry season for natural land use types.

HESSD
10, 15771–15809, 2013

3.5.3 Saturated zone

Apart from the net precipitation component ($P_e \times (1 - C_r)$), the saturated zone receives water from the unsaturated zone when the soil moisture S_u reaches field capacity ($S_{u,max}$). Excess overflow is routed to the groundwater using a recession factor, K_u. The saturated zone consists of three linear outlets which are separated by $S_{s,min}$ to represent the minimum storage level, $S_{s,q}$ to represent quickflow threshold and $S_{s,max}$ to represent rapid subsurface overflow. The flows are routed using K_o, K_q and K_s calibration coefficients respectively.

When the groundwater storage (S_s) exceeds the $S_{s,max}$, then saturation overland flow (Q_o) occurs:

$$Q_o = \max(S_s - S_{s,max}, 0)/K_o \quad (7)$$

where K_o is the overland flow recession constant.

The second groundwater flow component is the quick groundwater flow (Q_q). It is assumed to be linearly dependent on the S_s and a quick flow threshold $S_{s,q}$ determined through calibration (Eq. 8).

$$Q_q = \max(S_s - S_{s,q}, 0)/K_q \quad (8)$$

where K_q is the quick flow recession constant.

The third component is the slow groundwater flow (Q_s) which is dependent on the S_s levels

$$Q_s = (S_s)/K_s \quad (9)$$

where K_s is the slow flow recession constant.

K_o, K_s, K_q equal to 1, 2 and 28 respectively determined from recession curve analysis (where 1 unit is equal to 8 day).

The maximum saturation storage, ($S_{s,max}$) is a key variable that determines the dominant hydrological processes in the saturated zone. Three hydrological zones can be

HESSD
10, 15771–15809, 2013

delineated from $S_{s,max}$, i.e wetland, hill-slope and snow/ice zone. When $S_{s,max}$ is low, the saturation excess overland flow is dominant. This is characteristic for wetland system described in detail by Savenije (2010). It occurs in the low lying areas of the Pangani river basin where slopes are modest, or with shallow groundwater levels. During a rainfall event, there is no adequate storage of groundwater leading to saturation excess overland flow. The wetland system is therefore dominated by Q_o and as such the $S_{s,max}$ is set very low or at zero (fully saturated areas) and C_r at 1.

As the elevation and slope increases, the groundwater depth as well as the $S_{s,max}$ increase gradually. This is characteristic of the hill-slope system where storage excess subsurface flow is the dominant runoff mechanism. Topographic indicators can be used to identify and separate this zone from the wetland system (where $S_{s,max}$ is near zero). Recently developed indices that can be used include the elevation above the nearest open water (H) (Savenije, 2010), or the Height Above the Nearest Drainage (HAND) (Nobre et al., 2011; Cuartas et al., 2012). The first topographic indicator, H (elevation above the nearest open water) is used in this study. H is derived from the level where groundwater storage is low or near zero. This was estimated from 92 groundwater observation levels located on the lower catchments of the river basin (Fig. 4).

Figure 4 shows the delineation of the dominant hydrological processes in the Upper Pangani River Basin, including the wetland and hillslope (includes snowmelts at the peak of the mountains).

$S_{s,max}$ is not completely available for groundwater storage due to the soil texture (porosity and soil compression). According to Gerrits (2005), the maximum groundwater storage, $S_{s,max}$ [mm] for hillslope can be estimated using the natural log function of water storage depth, H_s (Eq. 10).

$$S_{s,max} = 25 \times \ln H_s \quad (10)$$

where H_s [m] is the normalized DEM above H (where (active) groundwater storage is assumed zero). It is noteworthy that the wetland system can still exist along the drainage network of river system beyond H. This is possible since the H_s would still

HESSD
10, 15771–15809, 2013

ensure a low groundwater storage ($S_{s,max}$) which makes the wetland system is the dominant hydrological process. As observed in Fig. 4, the middle catchment forms the transition from the wetlands to the hillslope. It is noted that the hydrological landscape, plateau (dominated by deep percolation and hortonian overland flow) described in detail by Savenije (2010) is forested in this river basin and is active in the rainfall–runoff process. It is therefore modeled as forested hillslope.

The third zone delineated is the snowmelt. The amount of snow in the river basin is limited to the small portion of the mountain peaks of Mt. Kilimanjaro and Mt. Meru. The snowmelt occurs at elevation ranges of 4070 m a.s.l. to 5880 m a.s.l. and is derived from the land use map (Kiptala et al., 2013a). During rainfall seasons, the snow is formed and stored in the land surface. During the dry season, the snow melts gradually to the soil moisture and to the groundwater. This is unlike the temperate climate where a lot of snow cover is generated during the winter seasons which may result in heavy or excess overland discharge during the summer seasons. Furthermore, Mt. Kilimajaro has lost most of its snow cover in the recent past due to climate variability/change, with significant snow visible only on the Kibo Peak (Misana et al., 2012). According to Grossmann (2008) the snowmelt contribution to groundwater recharge is insignificant in the Kilimanjaro aquifer. Simple representation of snowmelt can therefore be made using the hillslope parameters where the precipitation is stored in the unsaturated zone (C_r = 1 for snow) as excess unsaturated storage. The snowmelt is thereafter routed by K_u (unsaturated flow recession constant) to the groundwater over the season. This model conceptualization enables the hydrological model to maintain a limited number of parameters.

3.5.4 Interaction between the two zones

Capillary rise only occurs when groundwater storage is above a certain level the $S_{s,min}$. $S_{s,min}$ can be a fixed or a variable threshold value of the groundwater storage (S_s). Winsemius et al. (2006) adopted a fixed value of 25 mm as the $S_{s,min}$ for the Zambezi River basin. Since $S_{s,max}$ (from Eq. 10) is a function of H_s, a fixed threshold is not possible in

HESSD
10, 15771–15809, 2013

this study. $S_{s,min}$ is a function of groundwater storage S_s to provide a fixed but spatially variable (depends on H) value of $S_{s,min}$ through calibration over the river basin. Capillary rise above this threshold is estimated on the basis of the balance between water use needs at the unsaturated zone and water availability in the saturated zone. Actual capillary rise is determined by the maximum capillary rise C_{max} (calibration parameter for each land use type), actual transpiration T_a and the available groundwater storage S_s. Below the minimum groundwater level, $S_{s,min}$, a minimal capillary rise C_{min} is possible and is assumed to be zero for this study (timescale of 8 day is assumed low for substantial C_{min} to be realized).

$$C = \min(C_{max}, T_a, S) \rightarrow \text{if}(S_s \geq S_{min}) \quad (11)$$

where the active groundwater storage for capillary rise, $S = S_s - S_{s,min}$.

However, since the capillary flow is low compared to water use for some land use types, supplementary blue water from river abstractions Q_b is required in the system. The third blue water storage term S_d, is introduced to regulated blue water availability from capillary rise, C, and river abstractions, Q_b. River abstractions include water demands from supplementary irrigation, wetlands and open water evaporation for lakes or rivers derived directly from the river systems.

$$Q_b = (ET_b - C) \rightarrow \text{if} \quad (S_b \leq ET_b) \quad (12)$$

$$Q_b = 0 \rightarrow \text{if} \quad (S_b > ET_b) \quad (13)$$

where ET_b is the blue water required to fill the evaporation gap that cannot be supplied from the soil storage. For irrigated croplands, ET_b is assumed to represents the net irrigation abstractions in the river basin. The assumption is based on the 8 day timestep that is considered sufficient for the return flows to get back to the river systems, i.e. the flow is at equilibrium. The Q_b is therefore modeled as net water use in the river system. Since the river abstractions mainly occurs in the middle to lower catchments, the accumulation of flow would have a resultant net effect equivalent to the simulated discharge, Q_{sd} at the outlet point or gauging station.

HESSD
10, 15771–15809, 2013

3.6 Model performance

The modified STREAM model was calibrated and validated against measured daily discharge data from 5 gauging stations in the basin (see Fig. 1). One discharge gauge station, 1dd55, had a lot of missing data. Nevertheless, the limited information from this station, most upstream and the only one in the upper Mt. Meru, was useful in the calibration process of the downstream gauge stations. The daily discharge data were aggregated to 8 day time scale for the period 2008–2010. Since the secondary data from remote sensing (ET_a and f) were available for only 3 yr, 1 yr of data was used for calibration while the remainder of 2 yr data used for the validation.

The following goodness to fit statistics were used to evaluate the model performance. The Nash–Sutcliffe model efficiency coefficient (E) (Nash and Sutcliffe, 1970) in Eq. (14).

$$E = 1 - \frac{\sum_{i=1}^{n} (Q_s - Q_o)^2}{\sum_{t=1}^{n} (Q_o - \overline{Q}_o)^2} \quad (14)$$

where Q_s and Q_o are simulated discharge and observed discharge, $\overline{Q}_o$ is the mean of the observed discharge and n is the discharge data sets ($n = 46$ calibration; $n = 92$ validation). Since the model priority objective is to simulate low flows, the E_{ln} was also evaluated using natural logarithm of the variables in Eq. (14). The Mean Absolute Error (MAE) and Relative Root Mean Error (RMSE) Eqs. (15) and (16) metrics were also used to measure the average magnitude of errors between the simulated and observed discharges. In RMSE, the mean errors are square giving a relatively high weigh on

HESSD
10, 15771–15809, 2013

large errors compared to MAE.

$$\mathrm{MAE} = \frac{1}{n}\sum_{i=1}^{n}|Q_\mathrm{s} - Q_\mathrm{o}| \tag{15}$$

$$\mathrm{RMSE} = \sqrt{\frac{\sum_{i=1}^{n}(Q_\mathrm{s} - Q_\mathrm{o})^2}{n}} \tag{16}$$

The model estimates for blue water abstractions (Q_b) were also evaluated against field data for irrigation abstractions from the river basin agency, Pangani Basin Water Office.

4 Results and discussion

4.1 Calibration and validation results

Figures 5 and 6 show the comparison of the observed and simulated hydrographs and the average precipitation for 5 outlets (gauge stations) in the Upper Pangani River Basin. The figures provide a visual inspection of the goodness of fit of the data with an additional scatter plot for the most downstream outlet (1dd1). The model simulates the base flows very well both during the calibration and validation periods. The peak flows for the larger streams (1dd54, 1dd1) were better simulated than for the smaller streams (Figs. 5d and 6a). It is to be noted that the observed discharge data is also subject to uncertainty which is more pronounced for the smaller streams. The remotely sensed data, $\mathrm{ET_a}$ and f also have a higher uncertainty during the rainy season (peak flow season). This is the period when most clouded satellite images exist and the cloud removal process is subject to uncertainty (Kiptala et al., 2013b).

Table 1 shows the performance model results for the validation and calibration of the modified STREAM model in the Upper Pangani River Basin. E for the calibration period scored > 0.5 (except 1dd11a = 0.46) which is indicative of good model performance. In the validation period, two outlet points had scores < 0.5 (1dd11a – 0.33

HESSD
10, 15771–15809, 2013

and 1dd54 – 0.42) which indicates a moderate performance. E_{ln}, which emphasizes the base flow, resulted in better results with all outlet points scoring ≥ 0.6. There was a slight reduction in some outlet points but overall the model performance on the low flows was good.

MAE ranged between min. of 0.62 $m^3 s^{-1}$ to max. of 2.08 $m^3 s^{-1}$ for the larger streams in the calibration period. A big difference is observed between the RMSE and MAE (up to four times) for the downstream stations 1dd54 and 1dd1 during the calibration period. The result is indicative of large (noisy) variations between the simulated and observed discharges. Figure 5 shows that the large deviations arise during the rainy periods (Masika and Vuli seasons). This may be attributed to the uncertainties of the remote sensing data in the clouded periods (rainy days).

4.2 Interception

There is general consensus that interception (*I*) is a key component in hydrology and water management. Transpiration (*T*) influences the stream flow dynamics and the useful component of ET_a in biomass production. Therefore, there is a need to distinguish *T* from the calculated *I* as a deficit of total ET_a (SEBAL), Fig. 7.

The mean annual *I* ranged between 8–24 % of the total evaporation. The land use types in the upper catchments, e.g. forest, rainfed coffee and bananas, had higher *I*. Irrigated sugarcane and natural shrublands located on the lower catchments had lower *I*. The variation is mainly influenced by the *I* maximum threshold and the rainfall (intensity and frequency) which are relatively higher for land use types in the upper catchments. The forest interception average estimate of 24 % of the total evapotranspiration (or 22 % of the total rainfall) is comparable with field measurements from previous studies that found forest canopy interception of about 25 % of the total rainfall in a savannah ecosystem in Africa (Tsiko et al., 2012).

ET_b contributions, e.g. irrigation, also enhanced the transpiration (*T*) component of ET_a resulting in relatively lower *I* for irrigated croplands. Any intervention to change *I* would influence antecedent soil moisture conditions especially during small rainfall

HESSD
10, 15771–15809, 2013

events (Zhang and Savenije, 2005). This may influence the productivity of *T* or the stream flow generation in the river basin. However, more research is required to estimate explicitly the changes in *I* from certain field based interventions. The outcome of such studies maybe incorporated in the STREAM model.

4.3 Blue evapotranspiration

Figures 8c and 9 show the resultant blue evapotranspiration (ET_b) and the direct contribution of precipitation (ET_g) to the ET_a (total evaporation) for various land use types. ET_b is modeled to represent the contribution of blue water (irrigation abstraction or open water evaporation from rivers and lakes) to total evaporation (ET_a). ET_b is closely related to the land use and the ET_a as observed in Fig. 8a and b. Water bodies (lakes and reservoir) and the wetlands have the highest ET_b, contributed by the high open water evaporation. The average ET_b for water bodies is approximatey 56 % of the ET_a with a maximum of 74 % (1642 mm yr^{-1}) observed at the lower end of the NyM reservoir. The ET_b is high in the NyM reservoir because of the high potential evaporation contributed to hotter climatic conditions and lower precipitation levels in the lower catchments. Wetlands and swamps located in the lower catchments also resulted in high ET_b of approximately 42 % of ET_a. In irrigated croplands, the ET_b was also moderately high with a range of between 20 % for irrigated mixed crops and bananas in the upper catchments, and 44 % for irrigated sugarcane in the lower catchment.

Rainfed crops and natural vegetation including the forests had a lower ET_b, mainly stemming from groundwater (and snow melts). Sparse vegetation, bushlands, grasslands, natural shrublands had ET_b contributions of less than 1 % of total ET_a, while rainfed maize (middle catchments) and rainfed Coffee (upper catchments) had ET_b contributions of 2 % and 7 % of ET_a respectively. Dense forest and Afro-Alpine forest had slightly higher ET_b contributions (ranging between 7–9 %) attributed mainly to the availability of groundwater from snow melts in the upper mountains.

Notable higher ET_b was experienced in the dry year of 2009 (as shown by the error bars in Fig. 9). This is attributed to higher potential evaporation from relatively drier

HESSD
10, 15771–15809, 2013

weather conditions. The lower precipitation during this period also resulted in increased groundwater use for the afro-alpine and dense forest land uses in the upper catchments. For instance the ET_b contribution to ET_a for dense forest increased from 5 % in 2008 (a relatively wet year) to 10 % in 2009. The enhanced ET_b for the irrigated croplands during 2009 is also attributable to the higher potential evaporation and limited precipitation that increased the irrigation water requirement. This is illustrated by irrigated sugarcane where ET_b increased from 35 % in 2008 to 55 % in 2009. The ET_b for year 2010 were generally average for all land use types which is indicative of the average weather conditions that prevailed during the year.

4.4 Irrigation abstractions

This section presents the model results for supplementary irrigation water use ($Q_{b(I)}$ – irrigated croplands) as estimated at various outlet points (gauging stations) in the river basin. The annual irrigation abstractions, predominant during dry seasons, were accumulated and the average mean for the period 2008–2010 is presented in Fig. 10. Six gauge stations and three additional points (accumulation points for Kikuletwa, Ruvu and Lake Jipe) were also considered. The annual net irrigation (in million cubic meters) is converted to $m^3 s^{-1}$ to provide better comparison with the discharge data in Sect. 4.1.

The $Q_{b(I)}$ ranges from 0.06 $m^3 s^{-1}$ on the smaller streams to a total of 3.4 $m^3 s^{-1}$ and 4.2 $m^3 s^{-1}$ in the outlets of the Ruvu and Kikuletwa river systems respectively. A significant irrigation abstraction of 1.5 $m^3 s^{-1}$ was observed by the TPC sugarcane irrigation system, the largest single irrigation scheme in the river basin. The total $Q_{b(I)}$ upstream of NyM reservoir was estimated at 7.6 $m^3 s^{-1}$ which represents approx. 50 % of the low flows in the Upper Pangani River Basin.

Open canal irrigation is the commonly used irrigation technique in the Upper Pangani River Basin. There are an estimated 2000 small-scale traditional furrow systems, some 200–300 yr old (Komakech et al., 2012). According to records at the Pangani

HESSD
10, 15771–15809, 2013

Basin Water Office, approximately 1200 of these abstractions have formal water rights. PWBO estimates that the total gross irrigation abstraction is approx. 40 $m^3 s^{-1}$. The irrigation efficiencies of the irrigation systems range between 12–15 % (Zonal Irrigation office, Moshi). The field estimates provides net irrigation consumptions of approx. 6 $m^3 s^{-1}$ (using 15 % efficiency) and about 79 % of the $Q_{b(l)}$ model estimates. Here, we adopted higher irrigation efficiency limit of 15 % to compensate for any uncertainties that may arise from the higher irrigation efficiencies larger irrigation schemes. The capacity and ability of the river basin authority to monitor actual water abstraction is limited. However, considering these uncertainties, the model result was reasonably close to field estimates.

4.5 Open water evaporation

The blue water use by the water bodies ($Q_{b(w)}$) above NyM reservoir was also estimated using the modified STREAM model. $Q_{b(w)}$ is the net open water evaporation from blue water which would otherwise flow into the NyM reservoir. The water bodies considered include wetlands (98 km^2), Lake Jipe (25 km^2) and Lake Chala (4 km^2). The total mean $Q_{b(w)}$ were estimated to be 53.6 $Mm^3 yr^{-1}$ (1.7 $m^3 s^{-1}$) and 22.1 $Mm^3 yr^{-1}$ (0.7 $m^3 s^{-1}$) in the Ruvu and Kikuletwa river systems, respectively. The total $Q_{b(w)}$ (12 % of low flows) may also provide an insight into ecosystem services or benefits provided by the natural water bodies compared with the alternate uses e.g. irrigation or hydropower on the downstream of the river basin.

5 Conclusions

This paper presents a novel method of developing a spatially distributed hydrological model in a heterogeneous, highly utilized and data scarce landscape with a sub-humid and arid tropical climate. A distributed hydrological model, STREAM, was modified by employing a time series of remotely sensed evapotranspiration data as input. The

HESSD
10, 15771–15809, 2013

model was also constrained by satellite-based soil moisture estimates that provided spatially (and temporally) realistic depletion levels during the dry season. To further enhance model parameter identification and calibration, three hydrological landscapes; wetlands, hill-slope and snowmelt were identified using field data and observations. Unrealistic parameter estimates, found for example in natural vegetation either through overestimation of satellite-based data or model structure, were corrected in the model conceptualization through the water balance (at pixel level). The modified STREAM model provided considerably good representation of supplementary blue water use that is dominant in the river basin.

The model performed reasonably well on discharge, especially in the simulation of low flows. The E_{ln} ranged between 0.6 to 0.9 for all outlet points in both calibration and validation periods. Model performance was better for the larger streams compared with the smaller streams. The large difference between MAE and RMSE was indicative of large errors or noisy fluctuations (see Figs. 5 and 6) between actual and simulated discharges (in the rainy seasons). This was mainly attributed to the uncertainties of the remote sensing data in the clouded periods. The simulated net irrigation abstractions were estimated at 7.6 $m^3 s^{-1}$ which represents approximately 50 % of low flows. Model results compared reasonably well with field estimates with less than 20 % difference.

The model showed good potential for developing distributed models that can account for supplementary water use. In addition, the model yields spatially distributed data on net blue water use that provides insights into water use patterns for different landscapes, which can play a key role in water resources planning, water allocation decisions and in water valuation. The development of advanced methods of generating more accurate remotely sensed data, e.g. earth explorer, earth engine or cloud free algorithms such as ETLOOK (Bastiaanssen et al., 2012), should go hand in hand with ways to improve distributed hydrological models. In so doing, data can be interpreted in a way that is more useful for management and decision-making.

Acknowledgements. The research was funded by the Netherlands Ministry of Development Cooperation (DGIS) through the UNESCO-IHE Partnership Research Fund (UPaRF). It was

HESSD
10, 15771–15809, 2013

carried out in the framework of the Research Project "Upscaling small-scale land and water system innovations in dryland agro-ecosystems for sustainability and livelihood improvements" (SSI-2). We gratefully acknowledge data and information provided by the following organizations: Pangani Basin Water Office (Moshi, Tanzania), Tanzania Plantation Company – TPC (Moshi, Tanzania), Tanzania Meteorological Agency (Dar es Salaam, Tanzania) and Kenya Meteorological Department (Nairobi, Kenya).

References

Abwoga, A. C.: Modeling the impact of landuse change on river hydrology in Mara river basin, Kenya, Master's thesis, UNESCO-IHE Institute for Water Education, Delft, 2012.

Aerts, J. C. J. H., Kriek, M., and Schepel, M.: STREAM (Spatial tools for river basins and environment and analysis of management options): set up and requirements, Phys. Chem. Earth Pt. B, 24, 591–595, 1999.

Ahmed, M. D. and Bastiaanssen, W. G. M.: Retrieving soil moisture storage in the unsaturated zone from satellite imagery and bi-annual phreatic surface fluctuations, Irrigation Systems, 17, 3–18, 2003.

Allen, R. G., Tasumi, M., and Trezza, R.: Satellite based energy balance for mapping evapotranspiration with internalized calibration (METRIC): Model, ASCE J. Irrigation Drainage Engineering, 133, 380–394, 2007.

Bashange, B. R.: The spatial and temporal distribution of green and blue water resources under different landuse types in the Upper Pangani River Basin, Master's thesis, UNESCO-IHE Institute for Water Education, Delft, 2013.

Bastiaanssen, W. G. M., Menenti, M., Feddes, R. A., and Holtslag, A. A. M.: A remote sensing Surface Energy Balance Algorithm for Land (SEBAL) 1. Formulation, J. Hydrol., 212–213, 198–212, 1998a.

Bastiaanssen, W. G. M., Pelgrum, H., Wang, J., Ma, Y., Moreno, J. F., Roerink, G. J., and Van der Wal, T.: A remote sensing Surface Energy Balance Algorithm for Land (SEBAL) 2. Validation, J. Hydrol., 212–213, 213–229, 1998b.

Bastiaanssen, W. G. M., Cheema, M. J. M., Immerzeel, W. W., Miltenburg, I. J., and Pelgrum, H.: Surface energy balance and actual evapotranspiration of the transboundary Indus Basin

HESSD
10, 15771–15809, 2013

estimated from satellite measurements and the ETLOOK model, Water Resour. Res., 48, W11512, doi:10.1029/2011WR010482, 2012.
Campo, L., Caparrini, F., and Castelli, F.: Use of multi-platform, multi-temporal remote sensing data for calibration of a distributed hydrological model: an application in the Arno basin, Italy, Hydrol. Process. 20, 2693–2712, 2006.
Cuartas, L. A., Tomasella, J., Nobre, A. D., Nobre, C. A., Hodnett, M. G., Waterloo, M. J., de Oliveira, S. M., von Randow, R., Trancoso, R., and Ferreira, M.: Distributed hydrological modeling of a micro-scale rainforest watershed in Amazonia: model evaluation and advances in calibration using the new HAND terrain model, J. Hydrol., 462–463, 15–27, 2012.
De Groen, M. M. and Savenije, H. H. G.: A monthly interception equation based on the statistical characteristics of daily rainfall, Water Resour. Res., 42, W12417, doi:10.1029/2006WR005013, 2006.
FAO/IIASA/ISRIC/ISS-CAS/JRC: Harmonized World Soil Database (version 1.2), FAO, Rome, Italy and IIASA, Laxenburg, Austria, 2012.
Farr, T., Rosen, P., Caro, E., Crippen, R., Duren, R., Hensley, S., Kobrick, M., Paller, M., Rodriguez, E., Roth, L., Seal, D., Shaffer, S., Shimada, J., Umland, J., Werner, M., Oskin, M., Burbank, D., and Alsdorf, D.: The Shuttle Radar Topography Mission, Rev. Geophys., 45, RG2004, doi:10.1029/2005RG000183, 2007.
Fu, B., Wang, J., Chen, L., and Qiu, Y.: The effects of land use on soil moisture variation in the Danangou catchment of the Loess Plateau, China, Catena, 54, 197–213, 2003.
Gerrits, A. M. J.: Hydrological modelling of the Zambezi catchment from gravity measurements, Master's thesis, University of Technology, Delft, the Netherlands, 2005.
Gerrits, A. M. J.: The role of inetrception in the hydrological cycle, Ph.D. thesis, University of Technology, Delft, the Netherlands, 2010.
Grossmann, M.: Kilimanjaro Aquifer, in: Conceptualizing Cooperation for Africa's Transboundary Aquifer Systems, edited by: Scheumann, W. and Herrfahrdt-Pähle, E., DIE Studies Nr. 32, German Development Institute, 87–125, Bonn, 2008.
Immerzeel, W. M. and Droogers, P.: Calibration of a ditributed hydrological model based on satellite evapotranspiration, J. Hydrol., 349, 411–424, 2008.
Karssenberg, D., Burrough, P. A., Sluiter, R., and De Jong, K.: The PcRaster software and course materials for teaching numerical modelling in the environmental sciences, Transactions in GIS, 5, 99–110, doi:10.1111/1467-9671.00070, 2001.

HESSD
10, 15771–15809, 2013

Kiptala, J. K., Mohamed, Y., Mul, M., Cheema, M. J. M., and Van der Zaag, P.: Land use and land cover classification using phenological variability from MODIS vegetation in the Upper Pangani River Basin, Eastern Africa, J. Phys. Chem. Earth, 66, 112–122, 2013a.

Kiptala, J. K., Mohamed, Y., Mul, M. L., and Van der Zaag, P.: Mapping evapotranspiration trends using MODIS images and SEBAL model in a data scarce and heterogeneous landscape in Eastern Africa, Water Resour. Res., 49, 1–16, doi:10.1002/2013WR014240, 2013b.

Komakech, H. C., Van der Zaag, P., and Van Koppen, B.: The last will be first: water transfers from agriculture to cities in the Pangani River Basin, Tanzania, Water Alternatives, 5, 700–720, 2012.

Korres, W., Reichenau, T. G., Schneider, K.: Patterns and scaling properties of surface soil moisture in an agricultural landscape: an ecohydrological modeling study, J. Hydrol., 498, 89–102, 2013.

Liu, Y. B. and De Smedt, F.: WetSpa Extension, a GIS-Based Hydrologic Model for Flood Prediction and Watershed Management, Documentation and User Manual, Department of Hydrology and Hydraulic Engineering, Vrije Universiteit, Brussel, Belgium, 2004.

McDonnell, J. J., Sivapalan, M., Vache, K., Dunn, S., Grant, G., Haggerty, R., Hinz, C., Hooper, R., Kirchner, J., Roderick, M. L., Selker, J., and Weiler, M.: Moving beyond heterogeneity and process complexity: a new vision for watershed hydrology, Water Resour. Res., 43, W07301, doi:10.1029/2006WR005467, 2007.

Misana, S., Sokoni, C., and Mbonile, M.: Land-use/cover changes and their drivers on the slopes of Mount Kilimanjaro, Tanzania, Journal of Geography and Regional Planning, 5, 151–164, 2012.

Mohamed, Y. A., Bastiaanssen, W. G. M., and Savenije, H. H. G.: Spatial variability of evaporation and moisture storage in the swamps of the upper Nile studied by remote sensing techniques, J. Hydrol., 289, 145–164, 2004.

Nash, J. E. and Sutcliffe, J. V.: River flow forecasting through conceptual models, Part I: A discussion of principles, J. Hydrol., 10, 282–290, 1970.

Nelder, A. J. and Mead, R.: A simplex method for function minimization, Comput. J., 7, 308–313, 1965.

Nobre, A. D., Cuartas, L. A., Hodnett, M. G., Rennó, C. D., Rodrigues, G., Siveira, A., Waterloo, M. J., and Saleska, S.: Height above the nearest drainage – a hydrologically relevant new terrain model, J. Hydrol., 404, 13–29, 2011.

HESSD
10, 15771–15809, 2013

Norman, J. M., Kustas, W. P., and Humes, K. S.: A two-source approach for estimating soil and vegetation energy fluxes in observations of directional radiometric surface temperature, Agriculture for Meteorology, 77, 263–293, 1995.
Notter, B., Hurni, H., Wiesmann, U., and Abbaspour, K. C.: Modelling water provision as an ecosystem service in a large East African river basin, Hydrol. Earth Syst. Sci., 16, 69–86, doi:10.5194/hess-16-69-2012, 2012.
PBWO/IUCN: The Hydrology of the Pangani River Basin, Report 1: Pangani River Basin Flow Assessment Initiative, Moshi, 62 pp., 2006.
Rijtema, P. E. and Aboukhaled, A.: Crop water use, in: Research on Crop Water Use, Salt Affected Soils and Drainage in the Arab Republic of Egypt, Tech. rep., FAO, Near East Regional Office, Cairo, 5–61, 1975.
Roerink, G. J., Su, Z., and Menenti, M.: S-SEBI: A simple remote sensing algorithm to estimate the surface energy balance, Phys. Chem. Earth Pt. B, 26, 139–168, 2000.
Romaguera, M., Kros, M. S., Salama, M. S., Hoekstra, A. Y., and Su, Z.: Determining irrigated areas and quantifying blue water use in Europe using remote sensing Meteosat Second Generation (MSG) products and Global Land Data Assimilation System (GLDAS) data, Photogramm. Eng. Rem. S., 78, 861–873, 2012.
Ruhoff, A. L., Paz, A. R., Collischonn, W., Aragao, L. E. O. C., Rocha, H. R., and Malhi, Y. S.: A MODIS-based energy balance to estimate evapotranspiration for clear-sky days in Brazilian Tropical Savannas, Remote Sensing, 4, 703–725, 2012.
Savenije, H. H. G.: Determination of evaporation from a catchment water balance at a monthly time scale, Hydrol. Earth Syst. Sci., 1, 93–100, doi:10.5194/hess-1-93-1997, 1997.
Savenije, H. H. G.: Equifinality, a blessing in disguise?, Hydrol. Process., 15, 2835–2838, 2001.
Savenije, H. H. G.: The importance of interception and why we should delete the term evapotranspiration from our vocabulary, Hydrol. Process. 18, 1507–1511, 2004.
Savenije, H. H. G.: HESS Opinions "Topography driven conceptual modelling (FLEX-Topo)", Hydrol. Earth Syst. Sci., 14, 2681–2692, doi:10.5194/hess-14-2681-2010, 2010.
Scipal, K., Scheffler, C., and Wagner, W.: Soil moisture-runoff relation at the catchment scale as observed with coarse resolution microwave remote sensing, Hydrol. Earth Syst. Sci., 9, 173–183, doi:10.5194/hess-9-173-2005, 2005.
Seyfried, M. S. and Wilcox, B. P.: Scale and the nature of spatial variability: field examples having implications for hydrologic modeling, Water Resour. Res., 31, 173–184, 1995.

HESSD
10, 15771–15809, 2013

Shrestha, R., Tachikawa, Y., and Takara, K.: Selection of scale for distributed hydrological modelling in ungauged basins, IAHS-AISH P., 309, 290–297, 2007.
Su, Z.: The Surface Energy Balance System (SEBS) for estimation of turbulent heat fluxes, Hydrol. Earth Syst. Sci., 6, 85–100, doi:10.5194/hess-6-85-2002, 2002.
Tsiko, C. T., Makurira, H., Gerrits, A. M. J., and Savenije, H. H. G.: Measuring forest floor and canopy interception in a savannah ecosystem, Phys. Chem. Earth, 47–48, 122–127, 2012.
Uhlenbrook, S., Roser, S., and Tilch, N.: Hydrological process representation at the meso-scale: the potential of a distributed, conceptual catchment model, J. Hydrol., 291, 278–296, 2004.
Winsemius, H. C., Savenije, H. H. G., Gerrits, A. M. J., Zapreeva, E. A., and Klees, R.: Comparison of two model approaches in the Zambezi river basin with regard to model reliability and identifiability, Hydrol. Earth Syst. Sci., 10, 339–352, doi:10.5194/hess-10-339-2006, 2006.
Winsemius, H. C., Savenije, H. H. G., and Bastiaanssen, W. G. M.: Constraining model parameters on remotely sensed evaporation: justification for distribution in ungauged basins?, Hydrol. Earth Syst. Sci., 12, 1403–1413, doi:10.5194/hess-12-1403-2008, 2008.
Zhang, G. P. and Savenije, H. H. G.: Rainfall-runoff modelling in a catchment with a complex groundwater flow system: application of the Representative Elementary Watershed (REW) approach, Hydrol. Earth Syst. Sci., 9, 243–261, doi:10.5194/hess-9-243-2005, 2005.

HESSD
10, 15771–15809, 2013

Table 1. Model performance for the modified STREAM model for Upper Pangani River Basin.

Station	Calibration				Validation			
	E	E_{ln}	MAE ($m^3 s^{-1}$)	RMSE ($m^3 s^{-1}$)	E	E_{ln}	MAE ($m^3 s^{-1}$)	RMSE ($m^3 s^{-1}$)
1dc8a	0.63	0.68	0.73	0.92	0.72	0.68	0.62	0.36
1d5b	0.75	0.77	0.74	1.09	0.81	0.78	0.57	0.23
1dd11a	0.46	0.64	0.84	1.14	0.33	0.69	0.94	0.88
1dd54	0.70	0.60	2.31	8.06	0.42	0.61	1.99	5.84
1dd1	0.84	0.90	2.08	9.34	0.83	0.90	1.74	4.78

HESSD
10, 15771–15809, 2013

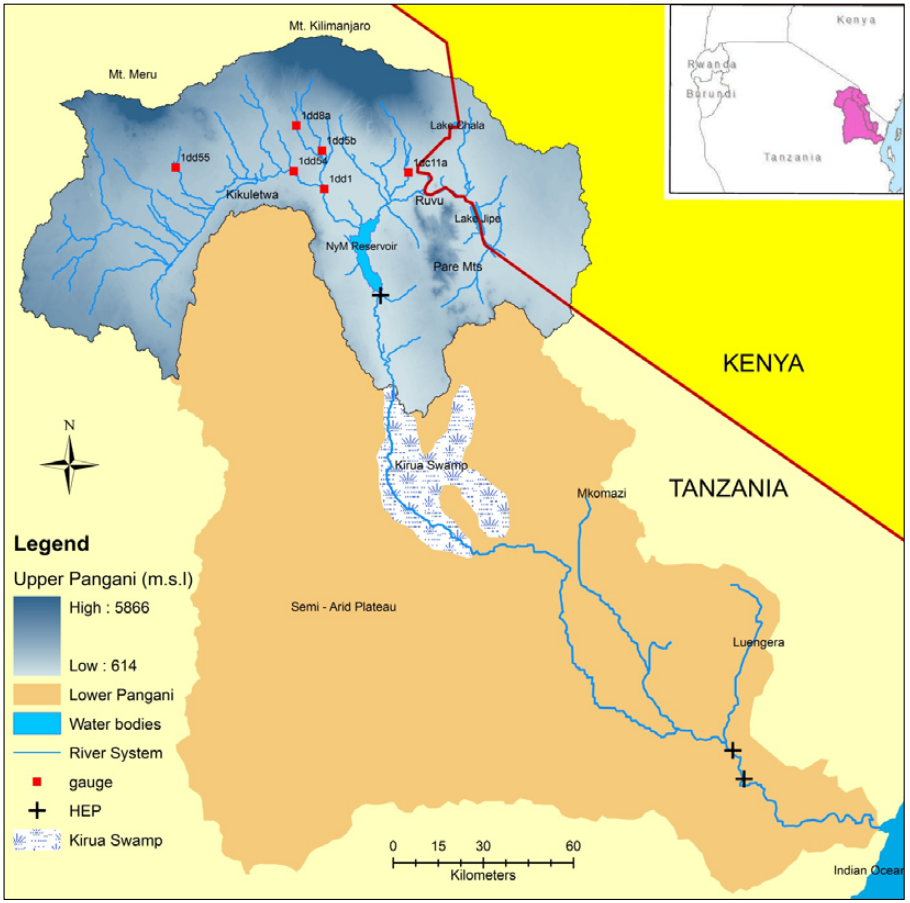

Fig. 1. Overview of entire Pangani River Basin and the Upper Pangani River Basin.

HESSD
10, 15771–15809, 2013




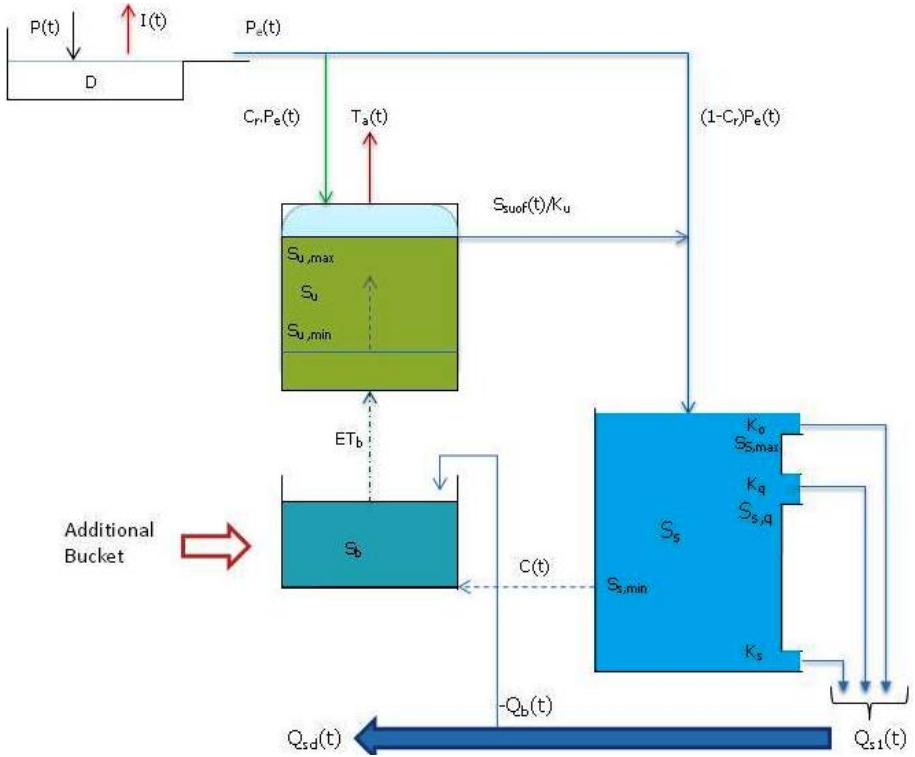

Fig. 2. Modified STREAM conceptual model for Upper Pangani River Basin.

HESSD
10, 15771–15809, 2013

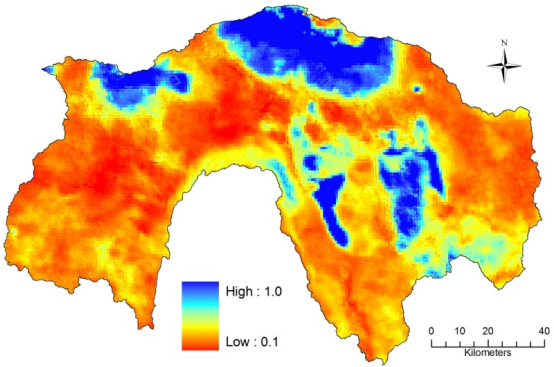

Land Use Type	Depletion fraction (f)
Water Bodies	0.87
Sparse Vegetation	0.27
Bushlands	0.29
Rainfed, Maize and Beans	0.30
Irrigation, Sugarcane	0.46
Irrigation; Bananas, coffee Maize	0.60
Dense Forest	0.72

Fig. 3. Soil moisture depletion fraction (defined using average values of the dry month of January of 2008, 2009 and 2010) in the Upper Pangani River Basin for selected land use types.

HESSD
10, 15771–15809, 2013

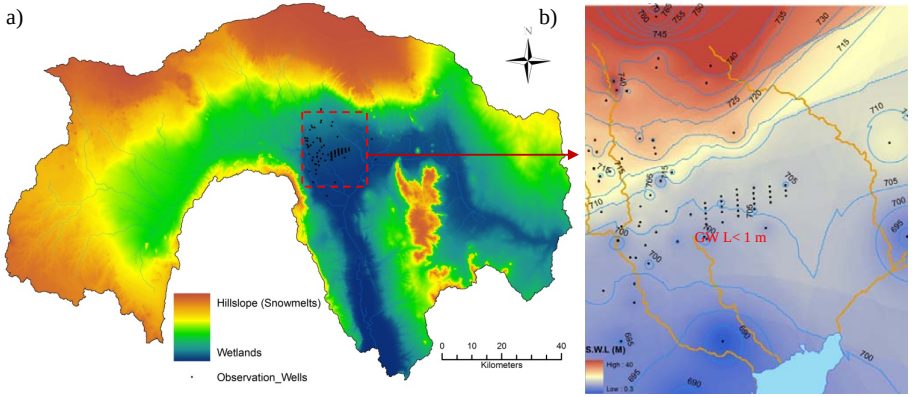

Fig. 4. (a) Wetland–Hillslope (Snowmelt) hydrological system **(b)** shallow groundwater observation wells with mean surface water levels (0.3–40 m) in the lower catchments of the Upper Pangani River Basin for the period 2008–2010.

HESSD
10, 15771–15809, 2013

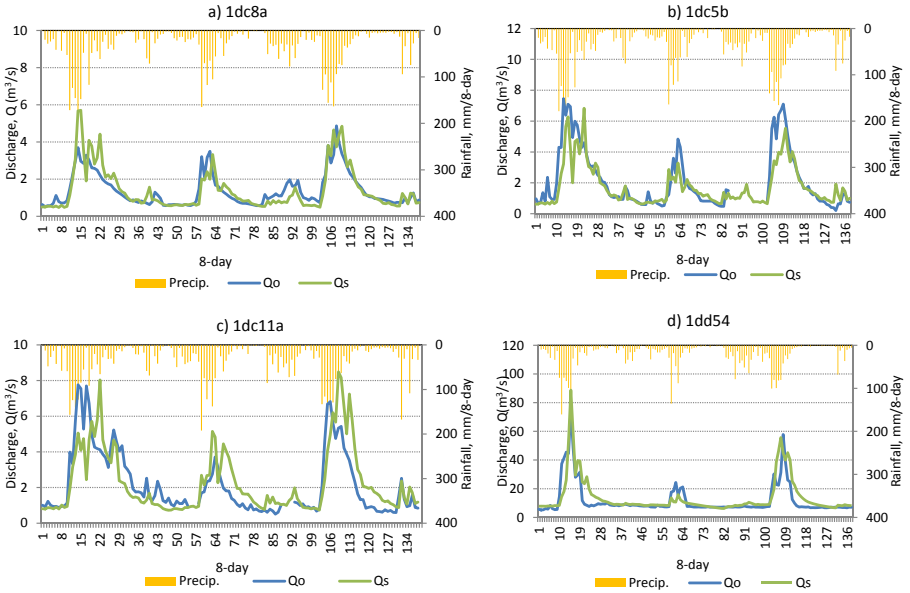

Fig. 5. (a–d) Comparison of observed (Q_o) and the simulated discharge (Q_s) and precipitation at the outlet points for calibration period 2008 (8 day periods 1–46) and validation 2009, 2010 (8 day periods 47–138) in the Upper Pangani River Basin.

HESSD
10, 15771–15809, 2013

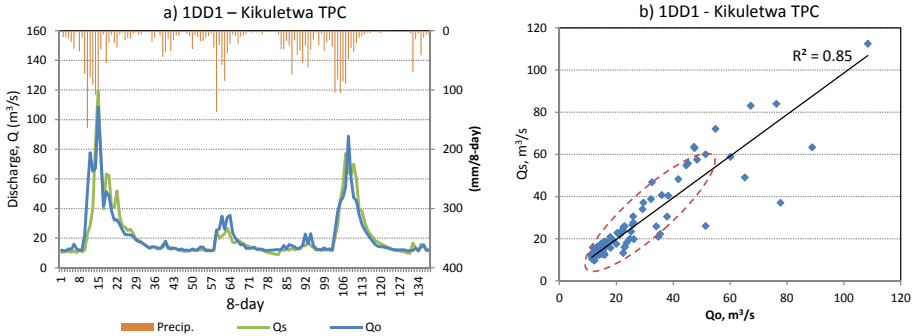

Fig. 6. (a) Comparison of observed (Q_o) and simulated discharge (Q_s) and precipitation for the most downstream outlet point for calibration period 2008 (8 day periods 1–46) and validation 2009, 2010 (8 day periods 47–138) in the Upper Pangani River Basin; and **(b)** the corresponding scatter plot of Q_o and Q_s.

HESSD
10, 15771–15809, 2013

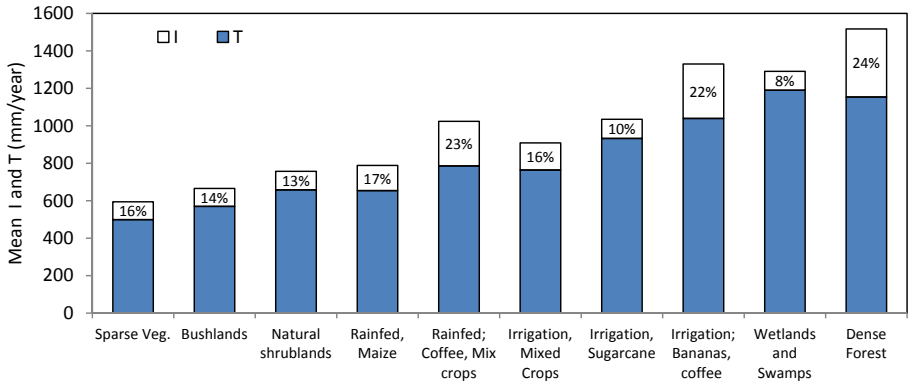

Fig. 7. Mean Interception, *I*, and mean transpiration, *T*, for different land use classes in Upper Pangani River basin for Period 2008–2010.

HESSD
10, 15771–15809, 2013

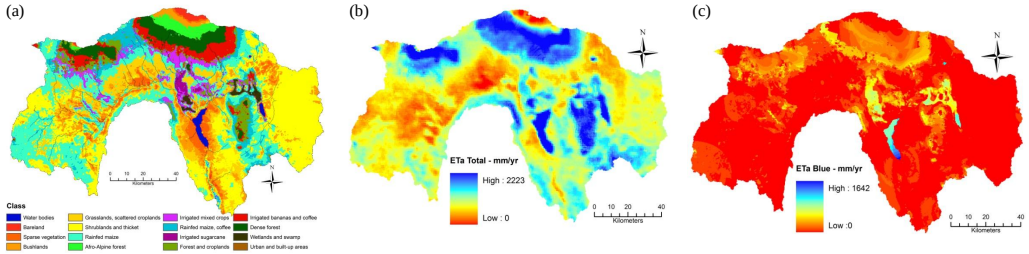

Fig. 8. Spatial Variability of **(a)** land use map (Kiptala et al., 2013a) **(b)** ET_a averaged for 2008–2010 (Kiptala et al., 2013b) and **(c)** ET_b averaged over 2008–2010 in the Upper Pangani River Basin.

HESSD
10, 15771–15809, 2013

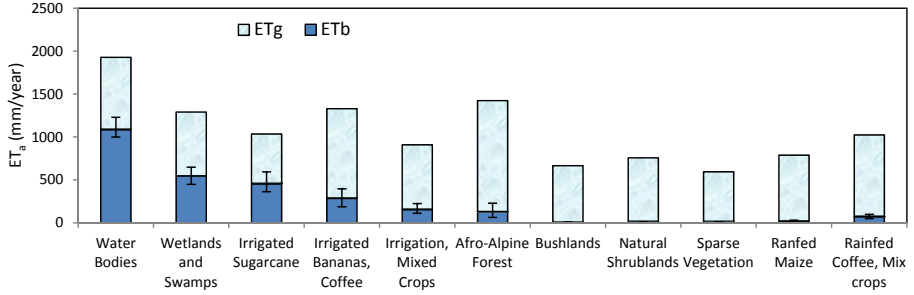

Fig. 9. ET_a and the corresponding ET_g and ET_b level for selected land use types averaged per year over 2008–2010 in the Upper Pangani River Basin (error bar indicates the upper and lower bounds for mean ET_b for dry year 2009 and wet year 2008 respectively).

HESSD
10, 15771–15809, 2013

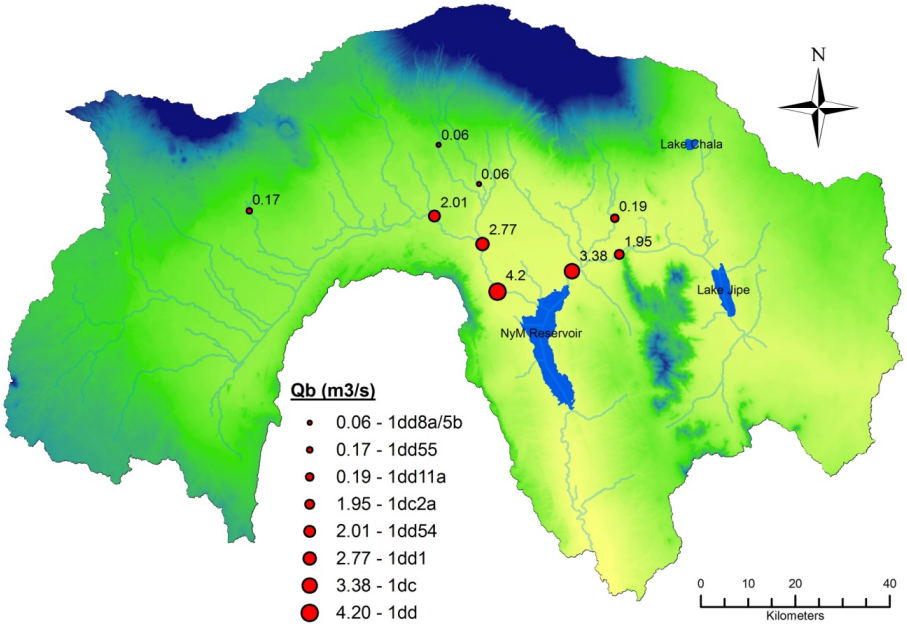

Fig. 10. Total net irrigation abstractions estimated upstream of the gauge stations using modified STREAM model in the Upper Pangani River Basin (averaged over years 2008–2010).

HESSD
10, 15771–15809, 2013